ISSN 1063-7834, Physics of the Solid State, 2015, Vol. 57, No. 7, pp. 1334–1341. © Pleiades Publishing, Ltd., 2015.
Original Russian Text © A.Yu. Stroeva, V.P. Gorelov, A.V. Kuz'min, V.G. Ponomareva, S.A. Petrov, 2015, published in Fizika Tverdogo Tela, 2015, Vol. 57, No. 7, pp. 1309–1314.

SEMICONDUCTORS

Effect of Iron Oxide on the Properties of $La_{0.9}Sr_{0.1}ScO_{3-\alpha}$ Protonics

A. Yu. Stroeva[a, *], V. P. Gorelov[a], A. V. Kuz'min[a, b], V. G. Ponomareva[c, d], and S. A. Petrov[c]

[a] *Institute of High Temperature Electrochemistry, Ural Branch of the Russian Academy of Sciences, ul. Akademicheskaya 20, Yekaterinburg, 620990 Russia*

[b] *Ural Federal University named after the First President of Russia B. N. Yeltsin, ul. Mira 19, Yekaterinburg, 620002 Russia*

[c] *Institute of Solid State Chemistry and Mechanochemistry, Siberian Branch of the Russian Academy of Sciences, ul. Kutateladze 18, Novosibirsk, 630128 Russia*

[d] *Novosibirsk National Research University, ul. Pirogova 2, Novosibirsk, 630090 Russia*

* *e-mail: stroevaanna@yandex.ru*

Received December 4, 2014; in final form, January 15, 2015

Abstract—The effect of doping on the transport properties of solid electrolytes $La_{0.9}Sr_{0.1}ScO_{2.95} + xFeO_{1.5}$ ($x = 0.1$–15.0 wt % $FeO_{1.5}$) has been elucidated by investigating the electrical conductivity of these materials by the four-probe method and the impedance method as a function of external parameters, namely, temperature T (150–900°C), oxygen partial pressure p_{O_2} (0.21×10^4–10^{-15} Pa), and humidity p_{H_2O} (0.04–2.35 kPa). Samples of the solid electrolytes have been investigated using X-ray powder diffraction, electron microscopy, and Mössbauer spectroscopy.

DOI: 10.1134/S1063783415070318

1. INTRODUCTION

In the development of electrolytes for solid oxide fuel cells (SOFCs) designed to operate at lower temperatures (500°C and below), proton-conducting solid electrolytes have undeniable advantages in comparison with oxygen electrolytes, because the activation energy of proton transfer is significantly less than that of oxygen ion transport, which provides substantially (by several orders of magnitude) higher conductivities under these conditions. On the other hand, materials with a mixed proton–electron conductivity as membranes for hydrogen production and electrode compositions for fuel cells are also of considerable interest [1].

Among the proton-conducting solid electrolytes, the highest hydrogen conductivity is observed in ABO_3 materials with a perovskite-type structure, including compounds with rare-earth cations A and B in the oxidation state of 3+. The acceptor doping of ABO_3 leads to an increase in the ionic conductivity, which in wet atmospheres is usually a mixed proton–oxygen conductivity [2, 3]. Among these compounds, the most interesting are the materials based on $LaScO_3$ [2–5]. The undoubted advantage of these materials, which is important for practical applications, is a higher chemical resistance as compared to the well-known proton-conducting solid electrolytes based on $SrCeO_3$ and $BaCeO_3$. An important characteristic of the materials based on $LaScO_3$ is their high bulk conductivity [4]. However, these materials possess high grain boundary resistances, which significantly decrease the total conductivity and represent serious obstacles to their use in practice. This problem also holds for other proton-conducting perovskites.

One way to eliminate grain boundary resistances of ceramic materials is to introduce dopants that could create a close intergrain contact and form highly conductive boundary phases.

In this work, we attempted to use the iron oxide $FeO_{1.5}$ as a sintering additive for the proton-conducting electrolyte $La_{0.9}Sr_{0.1}ScO_{2.95}$, which could compact intergrain contacts. On the other hand, the presence of $FeO_{1.5}$ in the material can lead to the formation of highly conductive boundary phases based on $LaFeO_3$ or $SrFeO_3$. At high concentrations, the $FeO_{1.5}$ dopants can lead to the formation of a membrane material with a proton–electron conductivity.

2. EXPERIMENTAL PART

2.1. Synthesis of Samples

Samples of the solid electrolytes $La_{0.9}Sr_{0.1}ScO_{2.95} + xFeO_{1.5}$, where $x = 0$, 0.1, 0.2, 0.5, 1, 5, 10, and 15 wt % (hereinafter, LSS, LSSF0.1, LSSF0.2, ..., LSSF15), were prepared by the ceramic method. The initial

materials used in the synthesis were as follows: La_2O_3 (special purity grade), Sc_2O_3 (OS-99), carbonyl iron, $SrCO_3$ (special purity grade 7–4), and nitric acid (reagent grade).

The samples of the specified composition were prepared by mixing in the required proportions of strontium carbonate, scandium oxide, and lanthanum oxide in zirconia mortar in an ethanol medium. A weighed portion of carbonyl iron was dissolved in a diluted HNO_3 (1 : 1) and then added to the mixture of oxides. The batch was calcined in air at a temperature of 1100°C for 1 h and then triturated in the dry air. The samples thus prepared were compacted without a binder in a steel mold under a pressure of 200 MPa. The final sintering of the molded samples was performed in air at a temperature 1600°C for 3 h.

2.2. Technique for Measuring the Electrical Conductivity

The electrical conductivity of the LSSF samples was measured by two methods: the direct-current (dc) four-probe method and impedance spectroscopy, depending on external parameters, namely, temperature T (150–900°C), oxygen partial pressure p_{O_2} (air—10^{-15} Pa), and humidity p_{H_2O} (0.04–2.35 kPa).

The four-probe method was used to measure temperature dependences of the electrical conductivity in the range of 500–900°C in air at two humidities (p_{H_2O} = 0.04 and 2.35 kPa). The measurements were carried out under cooling with a step of 10°C. The time of exposure at each temperature was 1 h. The measurements were performed on an automated setup, which made it possible to significantly increase the accuracy of the measurement: the electrical resistances R of the studied samples at each point were calculated with the special program from the slope of the current–voltage characteristic consisting of five points. The samples had the form of a parallelepiped 4 × 4 × 12 mm in size. Platinum electrodes were burned at a temperature of 1000°C for 1 h, followed by the activation with praseodymium oxide.

The impedance measurements of the electrical conductivity were performed using an IM6 Zahner Elektrik electrochemical complex and a Parstat 2273 potentiostat/galvanostat in the temperature range from 100 to 700°C at frequencies of up to 800 kHz with an alternating-current (ac) voltage amplitude of 10–30 mV at the samples with thicknesses of 0.9–1.2 mm.

The humidity of the air was set by the circulation of it through a bubbler with a controlled temperature of the water (p_{H_2O} = 0.61–2.65 kPa). The dry atmosphere (p_{H_2O} = 0.04 kPa) was created by the circulation of the air through columns filled with zeolites.

The oxygen partial pressures were produced by an electrochemical oxygen pump and controlled using an electrochemical sensor. The pump and sensor are fabricated based on the solid electrolyte YSZ (ZrO_2 + 8 mol % Y_2O_3). The experiments were carried out at the values of p_{O_2} in the range from the atmospheric oxygen partial pressure to 10^{-14} Pa.

The X-ray powder diffraction analysis was performed on a Rigaku DMAX 2200 X-ray diffractometer in the CuK_α radiation with a monochromator.

The scanning electron microscopy and microanalysis were carried out on a JSM 5900 LV scanning electron microscope with an INCA energy-dispersive spectrometer.

The Mössbauer spectra were measured at room temperature on an NZ-640 spectrometer (Hungary) operating in the constant acceleration mode with a reverse velocity and in the mode of a moving ^{57}Co radiation source in the metallic rhodium matrix. The chemical shifts are given relative to α-Fe. The spectra were processed with the original program of their decomposition into Lorentzian lines.

3. RESULTS AND DISCUSSION

3.1. Characterization of the Samples

The density of the sintered ceramic samples of LSS increases from 90 to 95% with an increase in the iron oxide content from 0 to 5 wt % $FeO_{1.5}$. In this case, the color of the samples is enhanced from gray to black. A further increase of the iron oxide content does not affect the density of the samples. The sintered samples have lustrous external surfaces and surfaces of cleavage. According to scanning electron microscopy, the grain size of the parent phase in the studied samples reaches 5 μm.

According to the X-ray diffraction data, samples of all the studied compositions have a perovskite-type structure with orthorhombic distortions. Since the principal lines of the Sc_2O_3 and $LaScO_3$ phases coincide with each other, the manifestation of a second phase in the X-ray diffraction patterns of the samples doped with 5 to 15 wt % $FeO_{1.5}$ can only be judged from the appearance of weak peaks assigned to Sc_2O_3 (Fig. 1). The SEM study and microanalysis of the samples doped with 1, 5, and 15 wt % $FeO_{1.5}$ demonstrated that the introduced iron, being a mineralogical analog of scandium, displaces it from the LSS lattice into an individual oxide phase, which clearly manifests itself upon doping even with 1 wt % $FeO_{1.5}$. This means that the lanthanum strontium ferrite $La_{0.90}Sr_{0.10}FeO_{2.95}$ is a more stable compound than the lanthanum strontium scandate $La_{0.90}Sr_{0.10}ScO_{2.95}$. Therefore, in the studied samples, there are two iron-containing phases, namely, the perovskite phase of mixed composition $La_{0.90}Sr_{0.10}Sc_{1-y}Fe_yO_{3-\alpha}$ and the

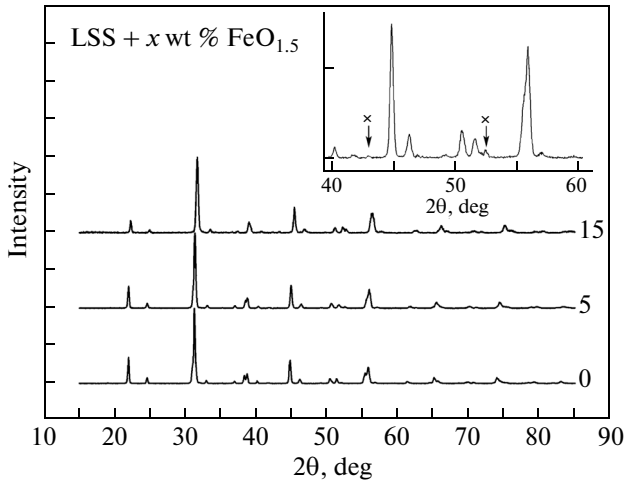

Fig. 1. Diffraction patterns of the $La_{0.9}Sr_{0.1}ScO_{2.95}$ + $xFeO_{1.5}$ samples with $x = 0$, 5, and 10 wt % $FeO_{1.5}$.

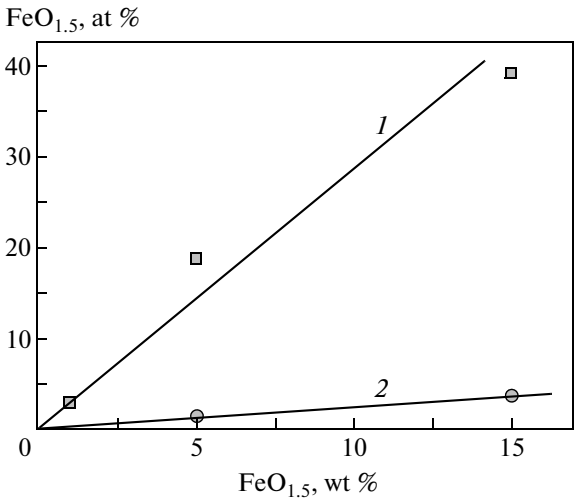

Fig. 2. Iron content in the coexisting phases: (*1*) the perovskite-type phase $La_{0.90}Sr_{0.10}Sc_{1-y}Fe_yO_{3-\alpha}$ and (*2*) the cubic phase based on scandium oxide $Sc_{0.995-z}Fe_zLa_{0.005}O_{1.5-\alpha}$.

cubic phases based on the scandium sesquioxide $Sc_{0.995-z}Fe_zLa_{0.005}O_{1.5-\alpha}$. The iron content in both phases increases in proportion to the addition of iron oxide to the samples (Fig. 2). However, iron is distributed between the two phases very nonproportionally: in the perovskite, the concentration of iron in the scandium sublattice is one order of magnitude higher than that in the scandium oxide phase. The latter phase, in addition to iron, contains a small amount of lanthanum (approximately 0.5 at %), but the presence of strontium is not revealed.

According to the results of the Mössbauer analysis, iron in the LSSF samples exists in two oxidation states, namely, Fe^{3+} and Fe^{4+}, which provides the migration of holes in the chains ($-Fe^{4+}-O^{2-}-Fe^{3+}-$) at high iron concentrations. At low concentrations (1 wt % $FeO_{1.5}$), iron predominantly exists in the oxidation state Fe^{4+} (Fig. 3). This confirms the well-known fact that the perovskite lattice tends to stabilize higher oxidation states of the cations [5]. With an increase in the iron content, the Fe^{4+} concentration in the samples decreases, whereas the Fe^{3+} concentration increases (Fig. 3).

3.2. Theory in Brief

The acceptor doping of $LaScO_3$ with Sr^{2+} cations embedded in the lanthanum sublattice implies the formation of substitutional cationic defects Sr'_{La} and oxygen vacancies $V_O^{\bullet\bullet}$ according to the quasi-chemical reaction (in the Kröger–Vink notation)

$$SrO(-LaO_{1.5}) \longrightarrow Sr'_{La} + 0.5V_O^{\bullet\bullet} + O_O^{\times}. \qquad (1)$$

Consequently, the dissolution of the iron oxide $FeO_{1.5}$ introduced into the stoichiometric $La_{0.9}Sr_{0.1}ScO_{2.95}$ protonic compound can occur according to the following reaction with the participation of oxygen vacancies and free interstitials $V_i^{\times}$ in the lattice:

$$FeO_{1.5} + 1.5V_O^{\bullet\bullet} + V_i^{\times} \longrightarrow Fe_i^{\bullet\bullet\bullet} + 1.5O_O^{\times}. \qquad (2)$$

According to this reaction, excess iron cations are located in the interstitial sites. Actually, taking into account the X-ray diffraction data on the displace-

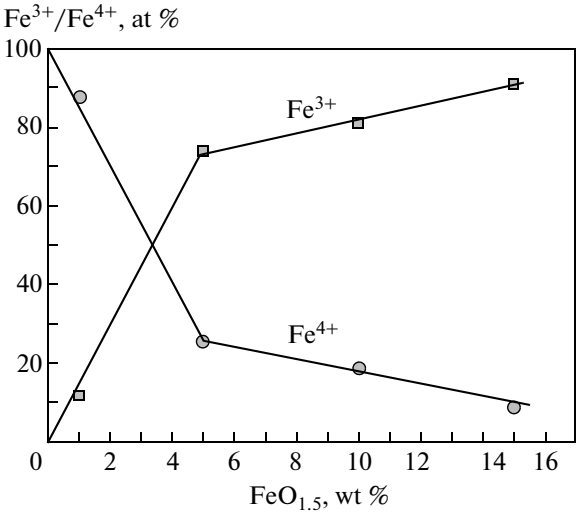

Fig. 3. Content of iron in the oxidation states of 3+ and 4+ in the $La_{0.9}Sr_{0.1}ScO_{2.95}$ + $xFeO_{1.5}$ samples according to Mössbauer spectroscopy.

ment of scandium by iron from the LSS lattice, the interstitial sites are occupied not by the iron cations but by the scandium cations:

$$FeO_{1.5} + 1.5V_O^{\bullet\bullet} + V_i^{\times} \longrightarrow Fe_{Sc}^{\times} + Sc_i^{\bullet\bullet\bullet} + 1.5O_O^{\times}. \quad (3)$$

The incorporation of highly charged cations $Sc_i^{\bullet\bullet\bullet}$ into the interstitial sites is energetically unfavorable. Indeed, upon doping of the sample even with 1 wt % $FeO_{1.5}$, the microanalysis revealed the precipitation of the second phase based on $ScO_{1.5}$.

The formation of protons $OH_O^{\bullet}$ localized on the oxygen ions $O_O^{\times}$ and proton conductivity in LSSF are caused by the interaction of oxygen vacancies with water vapor [6]:

$$V_O^{\bullet\bullet} + H_2O + O_O^{\times} = 2OH_O^{\bullet}, \quad (4)$$

$$[OH_O^{\bullet}] = K_4^{1/2}[V_O^{\bullet\bullet}]^{1/2}p_{H_2O}^{1/2}, \quad (5)$$

where K_4 is the equilibrium constant of reaction (4).

The interaction of oxygen vacancies with oxygen of the gas phase leads to the generation of electron holes $h^{\bullet}$ in the oxide and, consequently, to the hole conductivity:

$$V_O^{\bullet\bullet} + 1/2O_2 = 2h^{\bullet} + O_O^{\times}, \quad (6)$$

from which the hole concentration p in the oxide is determined by the formula

$$p = K_6^{1/2}[V_O^{\bullet\bullet}]^{1/2}p_{O_2}^{1/4}, \quad (7)$$

where K_6 is the equilibrium constant of reaction (6).

From the electroneutrality condition

$$[OH_O^{\bullet}] + 2[V_O^{\bullet\bullet}] + p = [Sr_{La}^{'}], \quad (8)$$

it follows that, in a dry atmosphere, the LSS compound will have only the hole–oxygen conductivity, whereas only the hole conductivity in this compound will be observed when the oxygen ion transport is hindered. In a hydrogen-containing reducing atmosphere, where the temperature dependence of the electrical conductivity has a plateau, the hole conductivity is absent and the electroneutrality condition is simplified:

$$[OH_O^{\bullet}] + 2[V_O^{\bullet\bullet}] = [Sr_{La}^{'}]. \quad (9)$$

From condition (9), it follows that, at high temperatures in a humidified atmosphere, the LSS oxides have a mixed proton–oxygen conductivity. However, at low temperatures, when the dissolved water vapor fill all the oxygen vacancies $V_O^{\bullet\bullet}$, the LSS oxides become purely proton-conducting electrolytes both in a reducing atmosphere and in an oxidizing atmosphere under the electroneutrality condition

Effective activation energies of the total conductivity E_{act} (±0.05 eV) of the LSSF samples for high-temperature (900–800°C) and low-temperature (650–540°C) sections of the curves at $p_{H_2O} = 2.35$ kPa

Composition	E_{act}, high-temperature section 900–800°C	E_{act}, low-temperature section 650–540°C
LSS	0.90	1.12
LSSF0.5	0.70	0.61
LSSF1	0.77	0.67
LSSF5	0.18	0.29
LSSF10	–0.09*	0.25
LSSF15	–0.06*	0.21

* The positive slope.

$$[OH_O^{\bullet}] = [Sr_{La}^{'}]. \quad (10)$$

The data on the D_2O solubility at 450°C in air, which were obtained using the nuclear microanalysis, confirmed that all oxygen vacancies are filled with water vapor [4].

3.3. Electrical Conductivity of LSSF Measured by the Four-Probe Method

All the temperature dependences of the electrical conductivity of the LSSF samples in the dry air at $p_{H_2O} \approx 0.40$ kPa and in the wet air at $p_{H_2O} = 2.35$ kPa have a curved shape in the Arrhenius coordinates. The effective conductivity activation energies E_{act} were calculated according to the formula $\log\sigma T = A\exp\{E_{act}/kT\}$ for high-temperature (900–800°C) and low-temperature (650–540°C) sections of the curves (see table), where the temperature dependences of the electrical conductivity can be considered to be linear (Figs. 4a, 4b). It turned out that the activation energies E_{act} obtained for the high-temperature and low-temperature sections of the curves decrease with an increase in the iron concentration, which indicates a regular increase in the electronic conductivity. A characteristic feature of the LSSF samples containing 5–15 wt % $FeO_{1.5}$ is a weak temperature dependence of the electrical conductivity: at low temperatures, the activation energy lies in the range of 0.3–0.2 eV, while at high temperatures, the slope of the curves for the LSS10 and LSS15 samples in the Arrhenius coordinates becomes even positive. In other words, the LSSF samples containing 5–15 wt % $FeO_{1.5}$ acquire properties typical of electron-conducting materials based on the lanthanum ferrite $LaFeO_3$, in which the migration of holes occurs in the chains $(-Fe^{4+}-O^{2-}-Fe^{3+}-)$ [7].

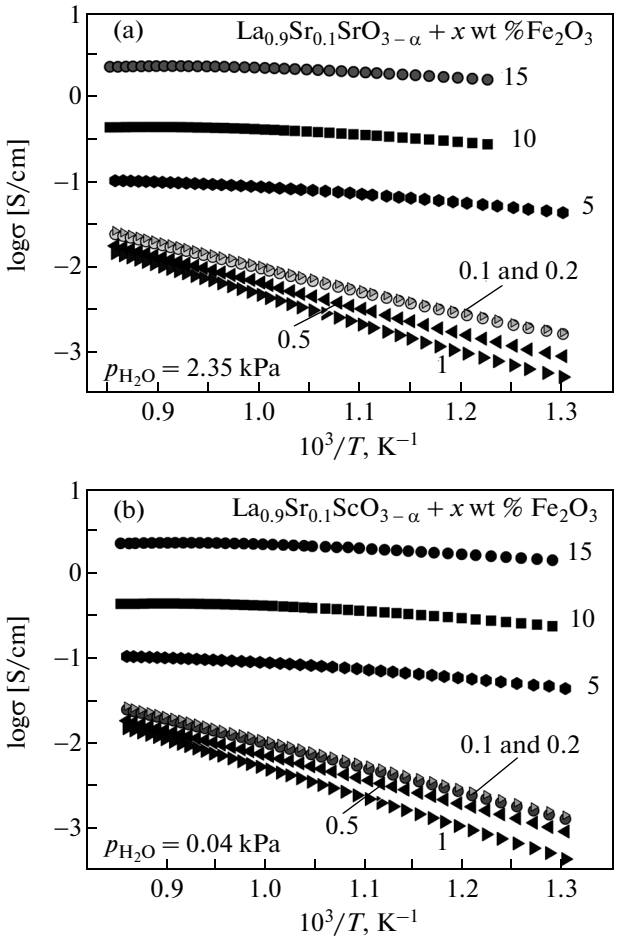

Fig. 4. Temperature dependences of the electrical conductivity of the LSSF samples at the air humidities p_{H_2O} = (a) 2.35 and (b) 0.04 kPa.

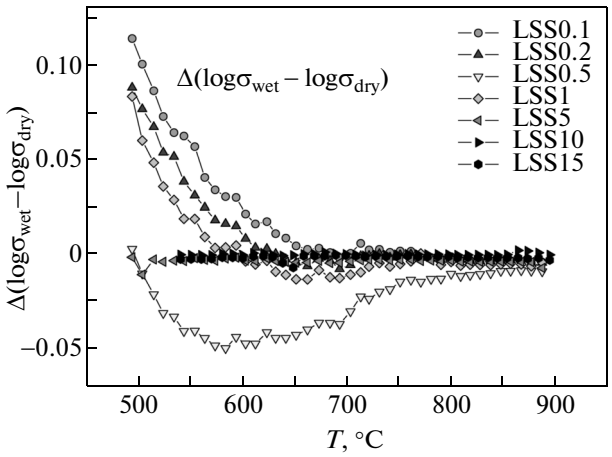

Fig. 5. Temperature dependences of the difference in the logarithms of the electrical conductivity in the wet air (p_{H_2O} = 2.35 kPa) and in the dry air (p_{H_2O} = 0.04 kPa).

3.4. Effect of the Air Humidity on the Electrical Conductivity of LSSF

Earlier [8–13], we found that, in the temperature range of 900–550°C, the humidity has little effect on the total conductivity σ_t of $LaScO_3$-based materials doped in one cation sublattice Sr'_{La} or in two cation sublattices Sr'_{La} and Mg'_{Sc}. A weak effect of the air humidity in the range p_{H_2O} = 0.04–2.35 kPa on the total conductivity is also observed for the studied LSSF materials (Figs. 4a, 4b).

In order to determined differences in the electrical conductivities of LSSF due to changes in the humidity, we determined the differences in the conductivities of the studied materials in the wet air at p_{H_2O} = 2.35 kPa and in the dry air at p_{H_2O} = 0.04 kPa (Fig. 5). It can be seen that the air humidity does not affect the electrical conductivity of the samples containing 5–15 wt % $FeO_{1.5}$: the difference between the electrical conductivities in the wet air and in the dry air is approximately equal to zero in the temperature range under investigation (Fig. 5). On this basis, we can conclude that the dissolution of the water vapor has no significant effect on the hole conduction implemented through the chains (–Fe^{4+}–O^{2-}–Fe^{3+}–).

With a decrease in the temperature, the solubility of the water vapor in the oxides increases, the concentration of protons also increases in the samples doped with small amounts of the iron oxide (0.1–1.0 wt % $FeO_{1.5}$), and an increase in the electrical conductivity is observed at temperatures below 600–650°C (Fig. 5), i.e., in the range of preferential proton conductivity for similar materials [8–13].

3.5. Electrical Conductivity of LSSF Measured by the Impedance Method

The measurements of the electrical conductivity of the studied materials by the impedance method in the temperature range of 600–150°C in an air atmosphere revealed that the total conductivity of $La_{0.9}Sr_{0.1}ScO_{2.95}$ remains unchanged upon doping with 0.1 and 0.2 wt % $FeO_{1.5}$ (Fig. 6). We could not separate the bulk and grain-boundary components of the conductivity by the impedance method: the extrapolation of the high-frequency semicircle of the impedance spectrum allowed us to determine only the total conductivity (Fig. 6, inset). The conductivity measured by the four-probe method in the range of 900–500°C was consistent with the data obtained by the impedance method for the total conductivity (Fig. 6).

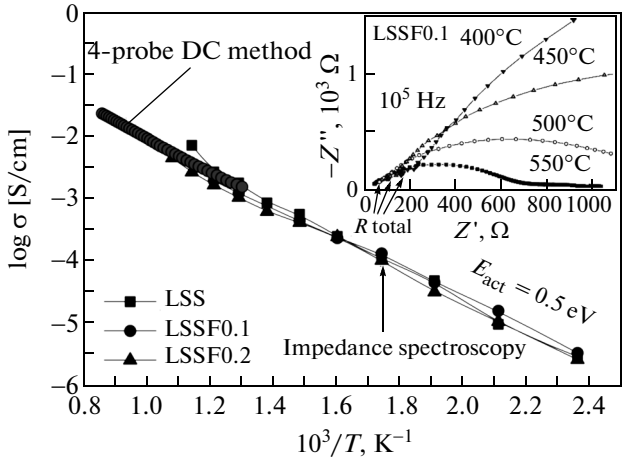

Fig. 6. Temperature dependences of the total conductivity in air at $p_{H_2O} = 2.35$ kPa, measured by the impedance method. The inset shows the frequency dependences for the LSSF0.1 sample at temperatures of 400–550°C.

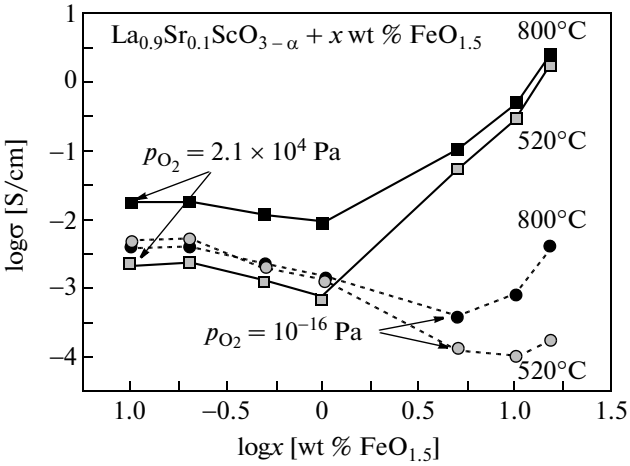

Fig. 7. Electrical conductivity isotherms of LSSF in an oxidizing atmosphere ($p_{O_2} = 0.21 \times 10^4$ Pa atm) and in a reducing atmosphere ($p_{O_2} = 10^{-16}$ Pa) at temperatures of 800 and 520°C and at the humidity $p_{H_2O} = 2.35$ kPa.

3.6. Concentration Dependences of the Electrical Conductivity of LSSF

Earlier, we showed that the dominant contribution to the total resistance of compounds in the $La_{1-x}Sr_xScO_{3-\alpha}$ and $La_{1-x}Sr_xSc_{1-y}Mg_yO_{3-\alpha}$ systems [8–13] comes from the grain boundaries. If small amounts of the iron oxide dopants (0.1 and 0.2 wt % $FeO_{1.5}$) do not affect the electrical conductivity of the LSS compounds, this means that they do not affect the electrical conductivity of the grain boundaries. Therefore, these iron oxide dopants are not present at the grain boundaries but are dissolved in the LSS lattice. On the other hand, such small amounts of the dopants also cannot significantly affect the electrical conductivity of the matrix (the conductivity of the grains) on the background of a large amount of the strontium acceptor dopant. As a result, the total conductivity of the sample does not change substantially.

However, the doping of the LSS samples with 0.5 and 1 wt % $FeO_{1.5}$ already significantly decreases their electrical conductivity (Fig. 7), which is explained by the precipitation of the poorly conducting scandium oxide at the grain boundaries. Based on data on the electrical conductivity, it can be concluded that, under the chosen synthesis conditions, the solubility limit upon doping with the iron oxide lies in the range between 0.2 and 0.5 wt % $FeO_{1.5}$.

A further increase of the iron oxide content in the samples above 1 wt % $FeO_{1.5}$ causes not a decrease but an increase in the electrical conductivity in air, which leads to the appearance of a minimum in the conductivity isotherms (Fig. 7). An increase in the electrical conductivity in this range of $FeO_{1.5}$ concentrations is rather significant: the conductivities of the LSSF1 and LSSF5 samples differ by almost one order of magnitude at a temperature of 900°C and by two orders of magnitude at 600°C. The measurements of the electrical conductivity as a function of the oxygen partial pressure p_{O_2} demonstrated that an increase in the electrical conductivity of the samples LSSF5–LSSF15 is caused by an increase in the hole conductivity (Fig. 8).

3.7. Effect of the Atmospheric Oxygen Partial Pressure on the Electrical Conductivity of LSSF

With a decrease in the oxygen partial pressure, the total conductivity σ_t of all the studied LSSF samples significantly decreases and, in reducing atmospheres, reaches a plateau (Fig. 8). Our previous investigations of the ion transport numbers by the electromotive force method demonstrated that, for the LSS sample, the plateau corresponds to a purely ionic (proton–oxygen) conductivity [12].

The observed decrease in the electrical conductivity with a decrease in the oxygen partial pressure p_{O_2} confirms that the studied materials have a hole conductivity under oxidizing conditions. The hole conductivity was determined as the difference between the total and ionic (on the plateau) conductivities under the assumption that the ionic conductivity σ_i does not depend on the value of p_{O_2} in the entire range of oxygen partial pressures, which is valid upon acceptor doping. The hole conductivity in these samples increases in proportion to $p_{O_2}^{1/4}$ in accordance with equation (7) at a constant humidity p_{H_2O}. An increase in the iron oxide content leads to an increase in the

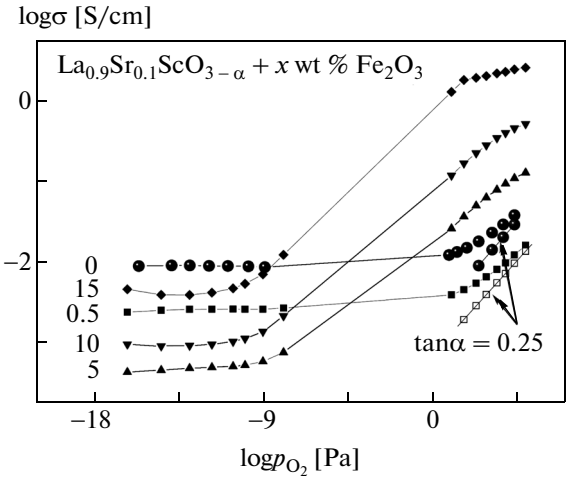

Fig. 8. Dependences of the electrical conductivity of LSSF0.5 on the oxygen partial pressure p_{O_2} at a temperature of 800°C and humidity $p_{H_2O} = 2.35$ kPa. The inclined straight lines show the hole conductivities of the LSS and LSSF0.5 samples (points are the experiment data, straight lines indicate the theoretical slope of 1/4).

contribution of the hole conductivity due to the migration of holes in the chains ($-Fe^{4+}-O^{2-}-Fe^{3+}-$). This type of hole conductivity weakly depends on in the oxygen partial pressure p_{O_2}. This is well illustrated by the LSSF15 sample, whose conductivity in oxidizing atmospheres increases in proportion with p_{O_2} to the 1/20 power (Fig. 8).

A clear plateau of the ionic conductivity, which was observed for samples in the previously studied systems $La_{1-x}Sr_xScO_{3-\alpha}$ and $La_{1-x}Sr_xSc_{1-y}Mg_yO_{3-\alpha}$ [8–13], is also observed in this study, except for LSS, only for the LSSF compounds doped with $FeO_{1.5}$ to 1 wt %. For the samples with a high iron oxide content (LSSF10 and LSSF15) in strongly reducing atmospheres after the plateau, there is an increase in the electrical conductivity due to the appearance of electronic conductivity in accordance with the reaction

$$O_O^\times = V_O^\bullet + 1/2O_2 + 2e'. \quad (11)$$

The electrical conductivity of LSSF in the region of the plateau in a reducing atmosphere decreases upon doping with iron oxide at a content of up to 5 wt % $FeO_{1.5}$ at 800°C and up to 10 wt % $FeO_{1.5}$ at 520°C (Fig. 8). This is associated with the low ionic conductivity of the phase based on scandium oxide, which precipitate at the grain boundaries. The observed increase in the electrical conductivity with a further increase in the iron oxide content is due to the phase transition of the scandium oxide at the grain boundaries into the highly conductive phase based on scandium ferrite.

4. CONCLUSIONS

The introduction of iron oxide dopants (0.1–15 wt % $FeO_{1.5}$) leads to the displacement of scandium from the lattice of the proton-conducting oxide $La_{0.9}Sr_{0.1}ScO_{2.95}$ (LSS), and the second phase based on scandium oxide is identified upon doping even with 1 wt % $FeO_{1.5}$. Iron is distributed between the two phases very nonproportionally: in the perovskite, the concentration of iron in the scandium sublattice is one order of magnitude higher than that in the scandium oxide phase.

According to the results of the Mössbauer analysis, iron in the samples exists in two oxidation states, namely, Fe^{3+} and Fe^{4+}, which provides the migration of holes in the chains ($-Fe^{4+}-O^{2-}-Fe^{3+}-$) at high iron concentrations. At low concentrations (1 wt % $FeO_{1.5}$), iron predominantly exists in the oxidation state Fe^{4+}.

The electrical conductivity of the samples was investigated by the four-probe method and the impedance method. The doping with iron oxide at contents beginning from 5 wt % $FeO_{1.5}$ leads to the formation of composites with a high hole conductivity in an oxidizing atmosphere. The electrical conductivity of LSS in a reducing atmosphere decreases upon doping with iron oxide up to contents of 5–10 wt % $FeO_{1.5}$. The dependences of the electrical conductivity on the oxygen partial pressure p_{O_2} demonstrate differences in the nature of charge transfer in the samples with small amounts of the dopants, which are characterized by the composition dependences typical of mixed ion–hole conductors doped with the iron oxide at a content above 5 wt % $FeO_{1.5}$, where the contribution from the hole conductivity increases several times.

ACKNOWLEDGMENTS

This study was supported by the Ural Branch of the Russian Academy of Sciences (project no. 12-S-3-1016 “Interface Conductivity in Solid Electrolytes for Fuel Cells”) and in part by the Russian Foundation for Basic Research (project no. 14-29-04013).

REFERENCES

1. K. Nomura and S. Tanase, Solid State Ionics **98**, 229 (1997).
2. D. Lybye and N. Bonanos, Solid State Ionics **125**, 339 (1999).
3. K. Nomura, T. Takeuchi, S. Kamo, H. Kageyama, and Y. Miyazaki, Solid Stdte Ionics **175**, 553 (2004).
4. V. P. Gorelov and A. Yu. Stroeva, Russ. J. Electrochem. **48** (10), 949 (2012).

5. S. Kemmler-Sack and I. Hofelich, Z. Naturforsch. **26** (6), 539 (1971).

6. K. D. Kreuer, Annu. Rev. Mater. Res. **33**, 333 (2003).

7. Y. Ren, R. Kungas, R. J. Gorte, and Ch. Deng, Solid State Ionics **212**, 47 (2012).

8. A. Yu. Stroeva, V. B. Balakireva, L. A. Dunyushkina, and V. P. Gorelov, Russ. J. Electrochem. **46** (5), 552 (2010).

9. A. Yu. Stroeva, V. P. Gorelov, and V. B. Balakireva, Russ. J. Electrochem. **46** (7), 784 (2010).

10. A. Yu. Stroeva, V. P. Gorelov, A. V. Kuz'min, V. B. Vykhodets, and T. E. Kurennykh, Russ. J. Electrochem. **47** (3), 264 (2011).

11. A. Yu. Stroeva, V. P. Gorelov, A. V. Kuz'min, E. P. Antonova, and S. V. Plaksin, Russ. J. Electrochem. **48** (5), 509 (2012).

12. A. Yu. Stroeva and V. P. Gorelov, Russ. J. Electrochem. **48** (11), 1079 (2012).

13. A. Yu. Stroeva, V. P. Gorelov, and B. D. Antonov, Russ. J. Electrochem. **48** (12), 1171 (2012).

Translated by O. Borovik-Romanova